Robotica (2005) volume 23, pp. 13–20. © 2005 Cambridge University Press
DOI: 10.1017/S0263574704000487 Printed in the United Kingdom

An improved energy stability margin for walking machines subject to dynamic effects

Elena Garcia* and Pablo Gonzalez de Santos

Instituto de Automatica Industrial, La Poveda, 28500 Madrid (Spain)
E-mail: egarcia@iai.csic.es

(Received in Final Form: April 26, 2004)

SUMMARY
Several static and dynamic stability criteria have been defined in the course of walking-robot history. Nevertheless, previous work on the classification of stability criteria for statically stable walking machines (having at least four legs) reveals that there is no stability margin that accurately predicts robot stability when inertial and manipulation effects are significant. In such cases, every momentum-based stability margin fails. The use of an unsuitable stability criterion yields unavoidable errors in the control of walking robots. Moreover, inertial and manipulation effects usually appear in the motion of these robots when they are used for services or industrial applications. A new stability margin that accurately measures robot stability considering dynamic effects arising during motion is proposed in this paper. The new stability margin is proven to be the only exact stability margin when robot dynamics and manipulation forces exist. Numerical comparison has been conducted to support the margin's suitability. Stability-level curves are also presented on the basis of a suitable stability margin to control the trajectory of the center of gravity during the support phase.

KEYWORDS: Walking robot; Stability margin; Static stability; Dynamic stability; Stability-level curves.

1. INTRODUCTION

There are more than one hundred and fifty walking machines already developed all over the world. Most of them are simple laboratory prototypes; however, there is a real need for walking machines. Legged locomotion has advantages on uneven terrain that make walking machines especially suitable for industrial and non-industrial applications, such as terrestrial and planetary exploration and humanitarian de-mining. Nevertheless, in order for successful real applications to be implemented, some problems must be solved, and the current performance of walking machines must be improved. In the last three decades legged locomotion has evolved at a breathtaking pace, but still one of the major shortcomings of walking robots is their poor speed. Some effort has been made to improve legged-locomotion speed by optimizing leg trajectories.[1] However, the optimization technique increases leg speed to close to the actuator-torque limits, and that proximity induces inertial effects that destabilize the robot's motion.

Walking robots that have been designed for industrial purposes perform statically stable gaits.[2–4] These robots are complex mechanisms featuring heavy limbs and the control of such limbs is challenging. The use of statically stable gaits enables their control to be simplified. However, if statically stable gaits are to be adopted, there must be no dynamic effects during motion, and thus these machines are limited to low, constant speeds to avoid inertial effects.

In the last two decades, the walking-robot community has displayed an increasing interest in the field of biped robots. Research on dynamic stability has focused on this particular design.[5–8] Although some dynamically stable quadrupeds exist, they are based on very simplified mechanisms, having only a few degrees of freedom, and adopt the stability criteria designed for bipeds, extended to a couple of additional legs.[9–11] The motion of these quadrupeds is limited to an even terrain, because the stability criterion used (Zero Moment Point) is only valid for that kind of surface, as some authors have demonstrated.[12–14]

Little effort has been made to cope with the dynamic effects that limit statically stable machines' performance.[15–19] However, one of the main goals of research on legged locomotion is the application of walking robots in industrial processes and services, and such robots are not meant to trot or gallop but to walk.

Recent research on the qualitative classification of stability margins for walking robots with more than two legs performing statically stable gaits has shown that currently there is a lack of stability margins to measure robot stability accurately when inertial and manipulation effects become involved.[20] These are precisely the dynamic effects that usually exist during the motion of walking robots in real services and industrial applications. Therefore, the main goal of this paper is to propose a new stability criterion for walking robots, performing statically stable gaits, whose stability margin accurately measures robot stability when inertial and manipulation effects exist. The proposed margin is an extension of the Energy Stability Margin[21] to the consideration of robot dynamics and therefore has been named **Normalized Dynamic Energy Stability Margin, NDESM**.

This paper is structured as follows: First, those stability criteria which are most related to the proposed one are briefly reviewed in Section 2. Next, the Normalized Dynamic

* Corresponding author

Energy Stability Margin is proposed in Section 3, and it is numerically compared with other stability margins in Section 4. The robot's stability-level curves are defined and plotted in Section 5, and finally, Section 6 presents some conclusions.

2. DEFINITION OF STABILITY MARGINS

In this section, the stability margins most related to the herein proposed one are defined. For a complete survey on static and dynamic stability margins see reference [20].

2.1. The Energy Stability Margin, ESM

The Energy Stability Margin, ESM, was proposed by Messuri[21] as the minimum potential energy required to tumble the robot around the edges of the support polygon, that is:

$$S_{ESM} = \min_{i}^{n_s}(mgh_i) \tag{1}$$

where i denotes the segment of the support polygon considered the rotation axis, n_s is the number of supporting legs, and h_i is the variation of CG height during the tumble, which comes from:

$$h_i = |\mathbf{R_i}|(1 - cos\,\theta)cos\,\psi \tag{2}$$

where R_i is the distance from the CG to the rotation axis, θ is the angle that R_i forms with the vertical plane, and ψ is the inclination angle of the rotation axis relative to the horizontal plane.

The ESM is the most effective static stability measurement. It gives a qualitative idea of the amount of impact energy the vehicle withstands and also considers the height of the CG. However, the ESM still does not consider any dynamic effects that might disturb vehicle stability. Extensions of the ESM were proposed by Nagy[22] to consider foot sinkage on soft and compliant terrain (the Compliant Energy Stability Margin, CESM) and the stabilizing effect of a leg of a foot that is in the air (the Tipover Energy Stability Margin, TESM). For most walking machines, the ESM and the TESM coincide because the non-supporting legs are too far from the floor to enhance stability. Only frame-based vehicles will find this stability margin an advantage.

2.2. The Normalized Energy Stability Margin, NESM

Hirose *et al.* normalized the ESM to the robot's weight and proposed the Normalized Energy Stability Margin, NESM, defined as.[23]

$$S_{NESM} = \frac{S_{ESM}}{mg} = \min_{i}^{n_s}(h_i) \tag{3}$$

The NESM was shown to be the most effective stability margin for statically stable walking machines. However, when dynamic effects arise during walking, machine stability cannot be judged precisely. Such situations exist in real walking robot applications, and therefore dynamic stability margins are more suitable.

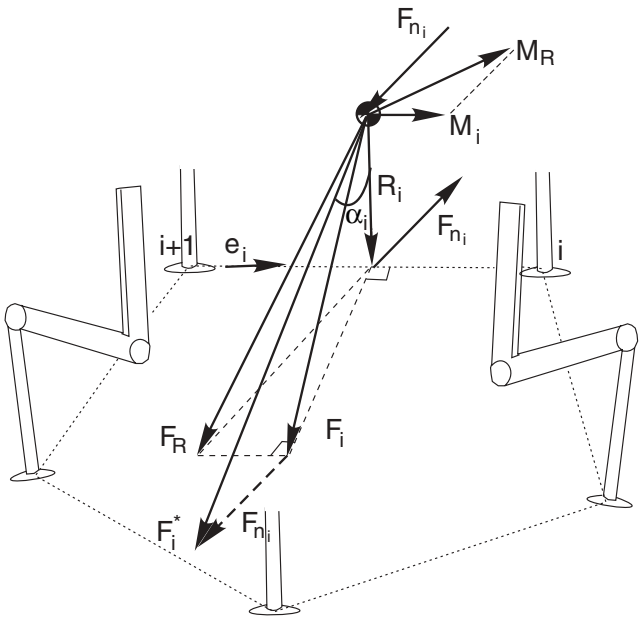

Fig. 1. Geometric problem of the Force-Angle stability margin.

2.3. Dynamic Stability Margin, DSM

To solve the unusefulness of static stability margins when robot dynamics are relevant some momentum-based stability criteria have been defined. Lin and Song[17] defined the Dynamic Stability Margin, DSM, as the smallest of all moments M_i around the edges of the support polygon caused by robot/ground interaction forces, normalized by the weight of the system, that is:

$$S_{DSM} = min_i\left(\frac{M_i}{mg}\right) = min_i\left(\frac{\mathbf{e_i}\cdot(\mathbf{F}_R \times \mathbf{P}_i + \mathbf{M}_R)}{mg}\right) \tag{4}$$

where P_i is the position vector from the CG to the *i-th* support foot, F_R and M_R are the resultant force and moment of robot/ground interaction, and $\mathbf{e_i}$ is a unit vector that revolves around the support polygon in the clockwise sense. If all moments are positive (if they have the same direction and sense as e_i), then the system is stable.

2.4. The Force-Angle Stability Margin, FASM

A different criterion was proposed by Papadopoulos and Rey.[18] The Force-Angle stability criterion finds the angle α_i between the resultant force acting from the CG on the ground (the opposite to the reaction force F_R) and the vector R_i, normal to the rotation axis from the CG (see Figure 1). The system becomes unstable when this angle becomes zero. The stability margin is the product of the angle times the resultant force F_R, that is:

$$S_{FASM} = min(\alpha_i)\cdot\|\mathbf{F}_R\| \tag{5}$$

These are the main stability criteria used for comparison with the herein proposed one. Recent research[20] has demonstrated that none of the static stability margins are suitable for measuring robot stability when robot dynamics are relevant. The FASM seems to be the best of the existing margins, because it accurately judges stability on flat terrain

https://doi.org/10.1017/S0263574704000487 Published online by Cambridge University Press

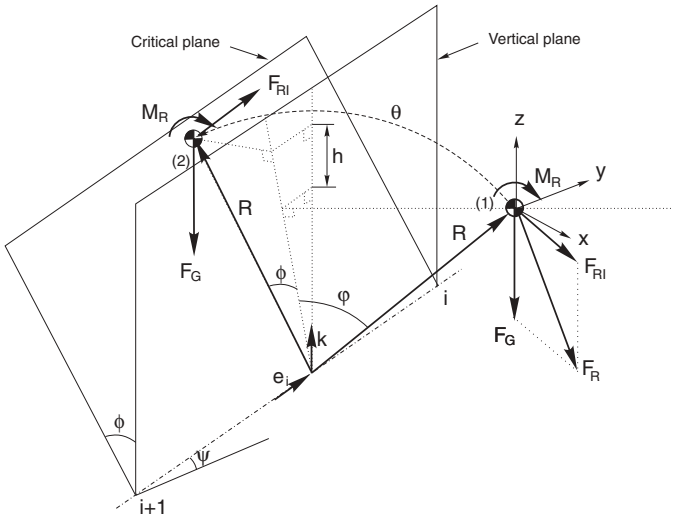

Fig. 2. Geometric outline for the computation of the NDESM.

in the presence of inertial effects. However, it loses accuracy when manipulation effects arise or when the robot walks over an uneven terrain. Furthermore, it shows that none of the dynamic stability margins accurately measure stability when there are manipulation forces and moments or dynamic effects during the transfer of the legs.

The following section of this paper is devoted to coping with this lack of accurate stability margins. A new margin is defined, which is shown to be the most accurate.

3. NORMALIZED DYNAMIC ENERGY STABILITY MARGIN

The optimum stability margin from the energy viewpoint is the one that quantifies the maximum impact energy that the machine can absorb without losing stability. Following this definition, the ESM is optimum under static conditions, e.g. when the only significant force acting on the robot is gravity, as previously demonstrated.[23] The ESM (see Section 2) is computed from the increase of potential energy that the machine's CG experiences when pivoting around the edges of the support polygon. Therefore, the extension of the ESM to the presence of other robot dynamics, like inertial forces or manipulation effects, must compute the increase of mechanical energy that the CG experiences during the tumble. This idea was proposed by Ghasempoor and Sepehri[24] to measure robot stability in the application to wheel-based mobile manipulators. In this paper, Ghasempoor and Sepehri's idea has been extended to walking machines, considering leg dynamics as a destabilizing effect.

Let us consider a walking robot during its motion, where gravitational, inertial and manipulation forces and moments become significant. At a given instant, an external impact causes the robot to tumble around one edge of its support polygon. The impact is caused by a force that interacts with the robot during an infinitesimal interval of time. Therefore, any joint motion during this interval is negligible and thus the robot will be considered as a rigid body. Figure 2 depicts the CG of a robot during the tumble around the edge of its support polygon, given by the line connecting footprints i and $i+1$. This edge is inclined at an angle ψ from the horizontal plane due to terrain inclination. If the moment around this rotational axis caused by the resultant forces and moments of robot/ground interaction, $\mathbf{F_R}$ and $\mathbf{M_R}$, is able to compensate for the destabilizing effect, the robot could maintain stability. If, on the contrary, the effect cannot be compensated for, the robot will lose stability. Therefore, the instant of critical stability occurs when the moment of robot/ground interaction forces and moments around the rotation axis vanishes. At that time the CG is located inside a **critical plane** that forms an angle ϕ with the vertical plane (see position (2) in Figure 2).

At the initial position (1) before the tumble, the CG is subject to inertial forces and moments ($\mathbf{F_I}$ and $\mathbf{M_I}$), gravitational forces and moments ($\mathbf{F_G}$ and $\mathbf{M_G}$), and manipulation forces and moments ($\mathbf{F_M}$ and $\mathbf{M_M}$). The perturbing effects of a leg in transfer phase can be also considered as manipulation terms. Assuming that the dynamics of the legs in the support phase is negligible relative to the body dynamics, the resultant force and moment of robot/ground interaction are given by:

$$\mathbf{F_R} = \mathbf{F_G} + \mathbf{F_M} - \mathbf{F_I} \tag{6}$$

$$\mathbf{M_R} = \mathbf{M_G} + \mathbf{M_M} - \mathbf{M_I} \tag{7}$$

During the tumble from position (1) to position (2), the gravitational force, $\mathbf{F_G}$, remains constant, while the rest of forces and moments rotate with the robot reference frame. Therefore, let us divide the resultant robot/ground interaction forces, $\mathbf{F_R}$, into two components: one gravitational and the other non-gravitational. Let us name the non-gravitational component $\mathbf{F_{RI}}$, that is:

$$\mathbf{F_{RI}} = \mathbf{F_R} - \mathbf{F_G} \tag{8}$$

The mechanical energy increase experienced by the CG during the tumble from position (1) to position (2) is given by the following energy balance:

$$E_i = V_2 - V_1 + K_2 - K_1 \tag{9}$$

where V_1 and K_1 are the potential and kinetic energies of the CG, respectively, before the tumble (1), and V_2 and K_2 are the potential and kinetic energy of the CG at the critical plane. Inside the critical plane the resultant moment around the rotation axis vanishes; thus the rotational speed of the CG is zero at this time, therefore:

$$E_i = V_2 - V_1 - K_1 \tag{10}$$

The increase of potential energy, $V_2 - V_1$, is the sum of potential energy due to gravity, $\mathbf{F_G}$, and the rest of forces and moments, $\mathbf{F_{RI}}$ and $\mathbf{M_R}$, that is:

$$V_2 - V_1 = \Delta V_G + \Delta V_F + \Delta V_M \tag{11}$$

$$\Delta V_G = mgh \tag{12}$$

$$\Delta V_F = \int_{\theta_1}^{\theta_2} (\mathbf{F_{RI}} \times \mathbf{R}) \cdot \mathbf{e_i}\, d\theta \tag{13}$$

https://doi.org/10.1017/S0263574704000487 Published online by Cambridge University Press

$$\Delta V_M = \int_{\theta_1}^{\theta_2} (\mathbf{M_R} \cdot \mathbf{e_i})\, d\theta \tag{14}$$

To compute the kinetic energy of the system before the tumble the following equation must be solved:

$$K_1 = \frac{1}{2} I_i \omega_i^2 \tag{15}$$

where I_i is the moment of inertia around the rotation axis, which is known, and ω_i is the angular speed of the robot before the tumble, which is obtained from:

$$\omega_i = \frac{L_i}{I_i} \tag{16}$$

Let us consider the speed of the CG before the tumble (1), $\mathbf{v}_{CG}$. Then, the angular momentum L_i is computed from:

$$L_i = (\mathbf{R} \times m\mathbf{v}_{CG}) \cdot \mathbf{e_i} \tag{17}$$

where m is the total mass of the robot and its manipulator system. Then the kinetic energy of the system before the tumble can be obtained by substituting equations (16) and (17) in (15).

Thus the term E_i in equation (9) is the increase of mechanical energy of the CG when pivoting around the edge i of the support polygon. It is also the increase of the machine's stability level when the machine is rotating around that axis due to an impulsive perturbation. Therefore let us propose the following definition:

Definition 3.1 *A walking machine is dynamically stable if every moment M_i around the i-edge of the support polygon due to robot/ground forces and moments is positive, with the vector that goes around the support polygon in the clockwise direction being positive, that is:*

$$M_i > 0, \quad i = 1..n-1 \tag{18}$$

where i is the edge of the support polygon, and n is the number of supporting feet. M_i is the moment around the axis i and comes from:

$$M_i = ((\mathbf{F_{RI}} + \mathbf{F_G}) \times \mathbf{R} + \mathbf{M_R}) \cdot \mathbf{e_i} \tag{19}$$

If equation (18) is true the robot is stable and then the **Normalized Dynamic Energy Stability Margin** is defined as:

Definition 3.2 ***The* Normalized Dynamic Energy Stability Margin, NDESM**, *is the smallest of the stability levels required to tumble the robot around the support polygon, normalized to the robot mass, that is:*

$$S_{MEEDN} = \frac{\min(E_i)}{mg} \tag{20}$$

where E_i is the stability level, given by (9).

The next section shows through simulation the improvement in stability margin measurement achieved using the proposed NDESM with different terrain profiles and dynamic effects.

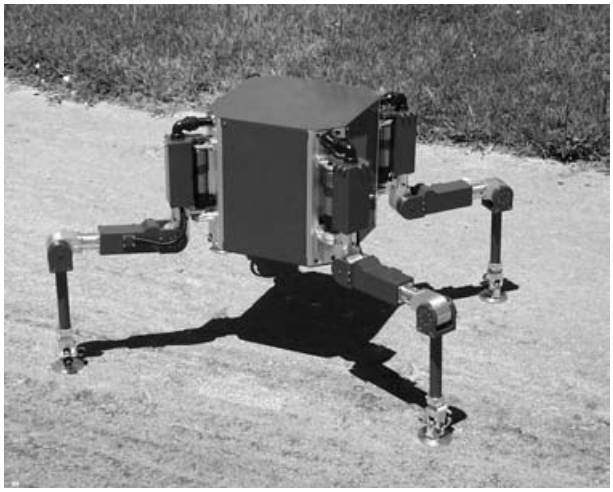

Fig. 3. The SILO4 walking robot.

4. VALIDATION OF THE NDESM

After defining the NDESM, this section analyzes how walking-robot stability measurement is improved using the stability margin herein proposed. A comparison between the NDESM and other classic stability margins is performed through numerical simulation of a walking robot in the following scenarios:

- Under static conditions.
- On inclined ground and subject to inertial and manipulation effects.

A commercial Simulation Construction Set (SCS)[25] was chosen for this purpose because it provides suitable tools for dynamic simulation. The SILO4 quadruped robot, shown in Figure 3, was used as a comparative testbed,[26] and the stability margins were computed while the robot was walking using a two-phase discontinuous gait.[27] Using the Java-based SCS library, robot kinematics and dynamics were defined as well as the ground profile and ground contact model. The integrator used for the simulation was based on the Runge-Kutta 4th-order method with an integration period of 0.4 ms. However, the data were collected for graphic comparison at a sampling time of 0.02 seconds.

Previous work on the classification of stability margins for walking machines[20] reveals that the FASM and the DSM are the most suitable stability margins when the robot is subject to dynamic effects. Therefore, in this paper the proposed NDESM is compared with the FASM and the DSM. Figure 4 shows numerical results, which are analyzed in the following subsections.

4.1. NDESM under static conditions

Under static conditions, the only force acting on the robot is gravity because $\mathbf{F_{RI}} = 0$ and $\mathbf{M_R} = 0$. Therefore the resultant robot/ground interaction force becomes:

$$\mathbf{F_R} = \mathbf{F_G} \tag{21}$$

https://doi.org/10.1017/S0263574704000487 Published online by Cambridge University Press

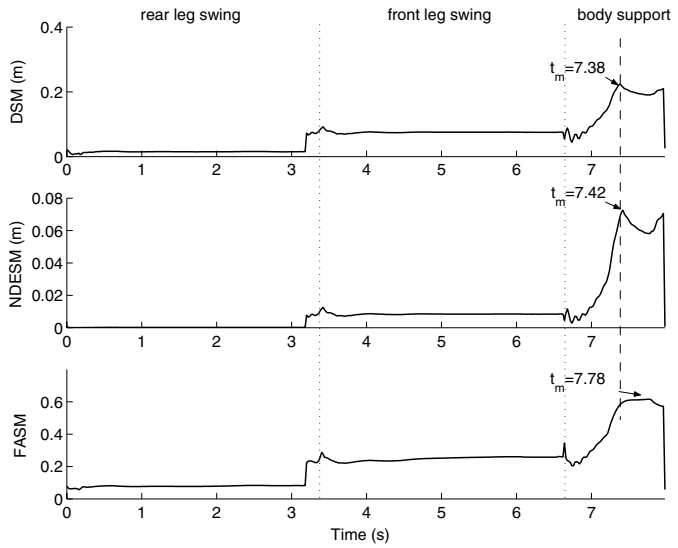

Fig. 4. DSM, NDESM and FASM during half a gait cycle when inertial and elastic effects arise and a 20-N manipulation force opposes robot motion on terrain inclined 10° from the horizontal plane.

Under such conditions, the critical plane coincides with the vertical plane, and the NDESM becomes:

$$S_{NDESM} = \min \frac{|\mathbf{R}|(1 - cos\,\theta)cos\,\psi}{mg} \tag{22}$$

The above expression of the NDESM matches the definition of the NESM (see equation 3). Therefore, under static conditions the NDESM and the NESM coincide. In such conditions, the NESM has been proved to be optimum,[23] therefore the NDESM is optimum too.

4.2. NDESM subject to inertial and manipulation effects

When the walking robot is subject to inertial effects due to its own body motion and manipulation effects caused by leg-transfer motion or robot-manipulator tasks, the NESM fails to measure robot stability. However, as Figure 4 shows, the NDESM is suitable for measuring robot stability under such conditions even on inclined ground. The DSM, NDESM, and FASM are represented during half a gait cycle, which consists of the transfer of the rear leg, followed by the transfer of the adjacent front leg, and lastly body propulsion. Figure 4 compares the three stability margins when the terrain is inclined 10 degrees and there are inertial effects added to a 20-N manipulation force perturbing the stability of a robot. Joint elasticity has been also considered. The vertical dashed line plotted inside the body support phase points to the instant when the DSM is maximum, and it is used for comparison of maximum-stability instants. Such instants of time have been written inside the figure for the sake of clarity.

This figure shows that the NDESM undergoes oscillations due to joint elasticity and reflects stability losses caused by inertia on the motion of the body and the legs during their transfer. The FASM and the DSM also undergo such modifications. However, when the robot is subject to manipulation forces the instant of maximum stability differs from one criterion to the other. In such a scenario the instant

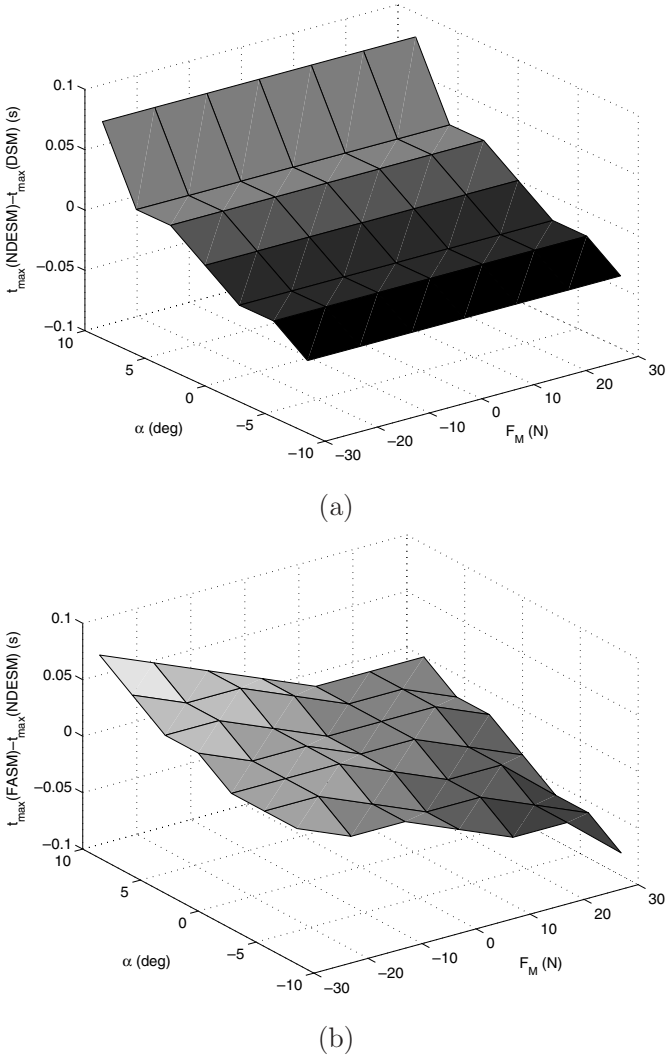

Fig. 5. Difference between instants of maximum stability for several terrain inclinations (α) and manipulation forces (F_M). (a) DSM vs. NDESM. (b) FASM vs. NDESM.

of maximum NDESM precedes the instant of maximum FASM and takes place after the instant of maximum DSM, as shown in Figure 4. These differences between the three stability margins persist for different terrain inclinations and manipulation forces. This is shown in Figures 5(a) and (b), where the instants of maximum DSM and FASM are compared with the instant of maximum NDESM for different terrain-inclination angles and different manipulation forces.

To determine which of the three stability margins is the best, an unstable situation has been simulated and stability margins have been computed. A 25-N external force opposing the robot's motion was simulated and the robot tumbled down. Dimensionless stability margins have been computed and scaled in order to permit numerical comparison. For this purpose, the NDESM has been divided by the robot height ($H = 0.34$ m), and the DSM has been divided by half the stroke pitch ($P/2 = 0.5$ m). Afterwards, the three dimensionless numbers have been scaled in such a way that at the beginning of the motion (when no external disturbances exist and the robot is stopped) they have the same value. It seems reasonable that under such normal

https://doi.org/10.1017/S0263574704000487 Published online by Cambridge University Press

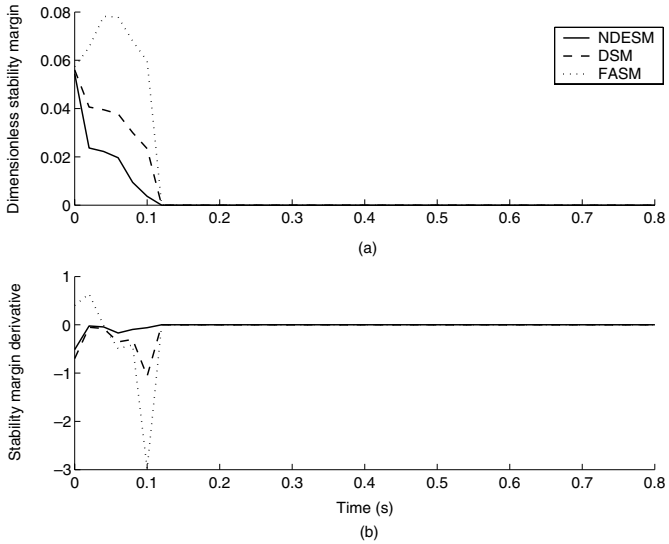

Fig. 6. (a) Dimensionless DSM, NDESM and FASM when instability takes place due to an external force of −25 N. (b) Dimensionless DSM, NDESM and FASM derivatives when instability takes place due to an external force of −25 N.

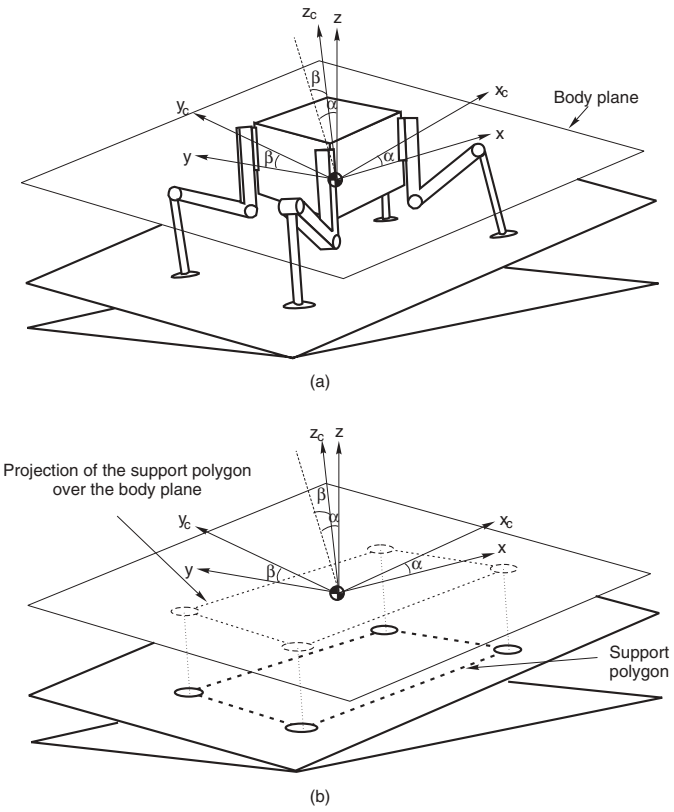

Fig. 7. Quadruped's body-support phase. (a) Body reference frame (x_c y_c z_c) and external reference frame (x y z). (b) Projection of the support polygon on the body plane.

conditions all dimensionless stability margins yield the same value. Figure 6(a) shows the three dimensionless stability margins before and after the tumble occurs (at $t = 0.1$ s). After the tumble the three stability margins become zero, just because the robot becomes unstable, and that prevents any stability margin to be computed. However, before the tumble, the three stability margins behave differently. The FASM reflects a delay in measuring the stability decrease just before the tumble, while the DSM and the NDESM show the stability decrease from the beginning of the motion. Nevertheless, the DSM exhibits a discontinuity at the instant of tumble. This is clarified in Figure 6(b), where derivatives of the three stability margins are shown. An impulse on derivatives of the DSM and FASM reveals an error in the instability prediction. These discontinuities do not seem to be so, due to the fact that the data shown in the figure has been sampled at $0.02s$ from the simulation data. However, stability margins become zero abruptly because when robot gets unstable no stability margin is computed (the support polygon disappears). However, if stability margins could have been computed, the FASM and the DSM surely would not have become zero, as shows the tendency of both curves in Figure 6(a) at that instant of time. As Figures 6(a) and (b) show, the NDESM becomes zero continuously, and thus no prediction error exists. Therefore, the NDESM has no error in the measurement of robot stability and can be used to predict robot instability precisely. This shows clearly the advantage of the NDESM which has been shown to be the only exact stability measurement. Just before the instant $t = 0.12$ s when the robot starts to fall, only the $NDESM = 0$. The rest of stability margins would give a margin different from zero. This is critical for robot control. If a robot gait is controlled in such a way that the stability margin must be always over a certain value, the use of other stability margin different from the NDESM will impose an error in the monitoring of the stability margin, and robot stability will be uncertain.

Therefore, the NDESM herein proposed is an improved stability measurement, that is able to predict robot stability precisely for different ground profiles and different dynamic effects perturbing motion, including robot inertia and manipulation dynamics.

5. STABILITY-LEVEL CURVES

Based on definition 3.2, the NDESM determines the maximum impact energy that the robot can absorb. If the support pattern remains fixed this amount of impact energy varies as the CG moves, e.g. during the body-support phase. Controlling the CG motion so as to guarantee a given stability level could be useful for the robot task because the maximum impact energy that can be absorbed would then be a known quantity.

In this section, stability-level curves are obtained inside the body plane (see Figure 7(a)) which is defined by the longitudinal and transverse robot axes (x_c and y_c) and the CG position. The stability-level curves are given by the following expression:

$$S_{NDESM}(x_c, y_c) = C \tag{23}$$

where x_c and y_c are CG coordinates with reference to a body reference frame x_c y_c z_c (see Figures 7(a) and (b)) and C is a constant. The support polygon and the forces and moments acting on the robot are known with reference to an external reference frame x y z.

https://doi.org/10.1017/S0263574704000487 Published online by Cambridge University Press

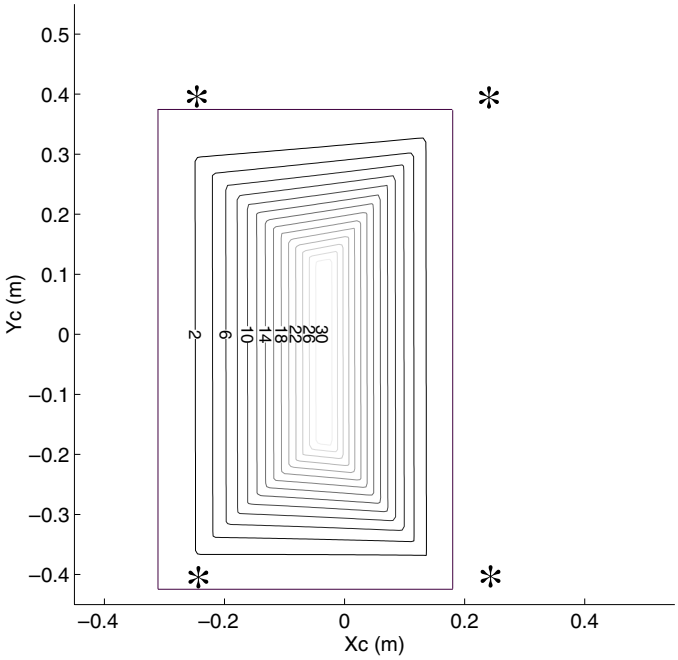

Fig. 8. Stability-level curves (m) over terrain inclined 20° in the x direction, horizontal body plane. The robot is subject to a 30-N manipulation force along the y-axis and a manipulation moment of 20 Nm around the y-axis.

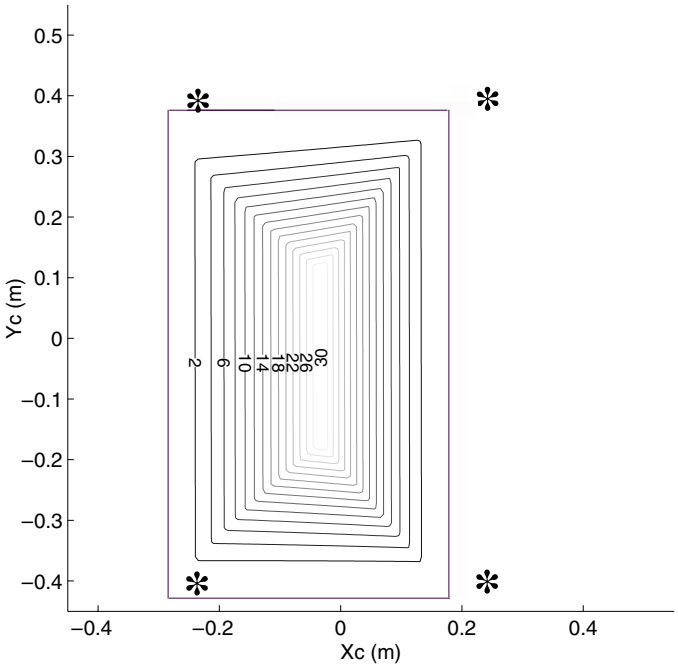

Fig. 9. Stability-level curves (m) over terrain inclined 20° in the x direction, horizontal body plane. The robot is subject to a 30-N manipulation force along the y-axis and a manipulation moment of 20 Nm around the y-axis, and the initial body speed is 0.2 m/s.

Let us name the position vector of the body reference frame in the external reference frame $\mathbf{G_0}$, that is:

$$\mathbf{G_0} = \left(x_{G_0}\ y_{G_0}\ z_{G_0}\right)^T \tag{24}$$

Any point in the body plane can be mapped into the external reference frame by means of the following homogeneous transformation:

$$\begin{pmatrix} x \\ y \\ z \\ 1 \end{pmatrix} = \begin{pmatrix} cos\,\alpha & sin\,\alpha sin\,\beta & sin\,\alpha cos\,\beta & x_{G_0} \\ 0 & cos\,\beta & -sin\,\beta & y_{G_0} \\ -sin\,\alpha & cos\,\alpha sin\,\beta & cos\,\alpha cos\,\beta & z_{G_0} \\ 0 & 0 & 0 & 1 \end{pmatrix} \cdot \begin{pmatrix} x_c \\ y_c \\ 0 \\ 1 \end{pmatrix} \tag{25}$$

where α is the angle between the x_c- and x-axes, and β is the angle between y_c- and y-axes (see Figure 7(b)).

Let us name the variable CG coordinates inside the body plane with reference to the external reference frame x_G, y_G, z_G:

$$\mathbf{G} = (x_G\ y_G\ z_G)^T \tag{26}$$

To solve equation (23) the NDESM must be expressed in terms of variable CG coordinates x_G, y_G, and z_G and later mapped onto the body reference frame through equation (25). As a result, the NDESM will be expressed in terms of body-plane coordinates x_c, y_c.

The analytic solution of (23) yields a complex expression. For the sake of clarity it has been solved numerically for different situations and results are plotted in Figures 8 and 9, which show stability-level curves for a quadruped in its support phase when dynamic effects are considered. Footprint projections onto the body plane are marked with an asterisk.

Figure 8 shows stability-level curves for a robot subject to a 30-N manipulation force along the y-axis and a 20-Nm manipulation torque around the y-axis. The robot remains at rest. The resultant force causes a moment around the x_c-axis, and therefore the critical plane forms an angle ϕ with the vertical plane for the two robot sides parallel to the x_c-axis. The zero-stability curve shifts from the support polygon due to this effect. Likewise, the manipulation torque around the y_c-axis causes the angle between the critical plane and the vertical plane for the two robot sides parallel to the y_c-axis. Manipulation forces and torques also modify the gradient between stability-level curves.

Also, stability-level curves are plotted for the same situation as in Figure 8 but while the robot is in motion, propelled by its four legs, that is, $V_{CG} \neq 0$. Under such conditions an initial kinetic energy exists. Figure 9 shows an example where the CG moves at a constant speed of 0.2 m/s along the x_c-axis. As a result, stability-level curves are squeezed in the x_c direction. Therefore robot stability decreases when the body moves.

6. CONCLUSIONS

Several static and dynamic stability criteria have been defined in the course of walking-robot history. Nevertheless, previous work on the analysis and classification of stability margins for walking machines with at least four legs has claimed that none of the existing stability margins have succeeded in measuring robot stability precisely when inertial and manipulation effects perturb the robot's motion. One of the main goals of research into legged locomotion is the application of walking robots in industrial processes and services, and

https://doi.org/10.1017/S0263574704000487 Published online by Cambridge University Press

such robots are usually subject to inertial and manipulation effects perturbing robot performance. Therefore, there is a need for accurate robot-stability measurement so that the current walking-machine performance can be improved.

In this paper, a new stability margin named NDESM has been proposed for walking robots with at least four legs. The NDESM is an extension of the NESM to account for the presence of inertial and manipulation effects acting on the robot's CG, and it determines the maximum impact energy that the robot can absorb. In this paper, it has been shown that the proposed NDESM is the only stability margin that provides an accurate stability measurement in the presence of robot dynamics and manipulation effects. This means that the measure it provides is exact, that is, if the $NDESM = 0$ at instant t, then the robot will start to fall at instant t. The advantage of using the NDESM for robot control has been shown. At the instant of time when the robot starts to fall, only the $NDESM = 0$. The rest of stability margins give a margin different from zero and thus, the control of robot stability will be uncertain.

Using the improved stability margin herein proposed, stability-level curves have been obtained for a robot in different dynamic situations on inclined terrain. The computation of stability-level curves enables CG location to be controlled inside the body plane such as to achieve a certain stability level. The use of the NDESM and stability-level curves for gait control will play a major role in the successful generation of walking-robot tasks.

Acknowledgements

The authors want to thank Jerry Pratt for his help using the simulation software package.

This work has been partially funded by CICYT (Spain) through Grant DPI2001-1595. The Community of Madrid sponsored a scholarship granted to the first author for this work.

References

1. E. Garcia and P. Gonzalez de Santos, "Using soft computing techniques for improving foot trajectories in walking machines," *Journal of Robotic Systems* **18**(7), 343–356 (2001).
2. V. Kumar and K. Waldron, "A review of research on walking vehicles," **In**: (O. Khatib, J. J. Craig and T. Lozano-Perez, editors) *The Robotics Review* (The MIT Press, Cambridge, Massachusetts, 1989) pp. 243–266.
3. R. McGhee and A. Frank, "On the stability properties of quadruped creeping gaits," *Mathematical Bioscience* **3**, 331–351 (1968).
4. S. Song and K. Waldron, *Machines That Walk: The adaptive suspension vehicle* (The MIT Press, Cambridge, Massachusetts, 1989).
5. S. Arimoto and F. Miyazaki, "Biped locomotion robots," *JARECT Computer Science and Technologies* **12**, 194–205 (1984).
6. K. Hirai, M. Hirose, Y. Haikawa and T. Takenaka, "The development of Honda humanoid robot," *Proc. IEEE Int. Conf. Robotics and Automation*, Leuven, Belgium (May, 1998) pp. 1321–1326.
7. K. Löffler, M. Gienger and F. Pfeiffer, "A biped jogging robot – theory and realization," *Proc. Int. Conf. Climbing and Walking Robots*, Madrid, Spain (October, 2000) pp. 51–58.
8. M. Raibert, *Legged Robots That Balance* (The MIT Press, Cambridge, Massachusetts, 1986).
9. M. Buehler, R. Battaglia, A. Cocosco, G. Hawker, J. Sarkis and K. Yamazaki, "Scout: A simple quadruped that walks, climbs and runs," *Proc. IEEE Int. Conf. Robotics and Automation*, Leuven, Belgium (May, 1998) pp. 1701–1702.
10. M. Raibert, M. Chepponis and H. Brown Jr., "Running on four legs as though they were one," *IEEE Journal of Robotics and Automation* **RA2**(2), 70–82 (1986).
11. H. Wong and D. Orin, "Dynamic control of a quadruped standing jump," *Proc. IEEE Int. Conf. Robotics and Automation*, Atlanta, Georgia (1993) pp. 346–351.
12. A. Goswami, "Postural stability of biped robots and the foot-rotation indicator (fri) point," *Int. J. Robotics Research* **18**(6), 523–533 (1999).
13. H. Kimura, I. Shimoyama and H. Miura, "Dynamics in the dynamic walk of a quadruped robot," *Advanced Robotics* **4**(3), 283–301 (1990).
14. K. Yoneda, H. Iiyama and S. Hirose, "Intermitent trot gait of a quadruped walking machine dynamic stability control of an omnidirectional walk," *Proc. IEEE Int. Conf. Robotics and Automation*, Atlanta, Georgia (1996) pp. 3002–3007.
15. P. Gonzalez de Santos, M. Jimenez and M. Armada, "Dynamic effects in statically stable walking machines," *Journal of Intelligent and Robotic Systems* **23**(1), 71–85 (1998).
16. D. Kang, Y. Lee, S. Lee, Y. Hong and Z. Bien, "A study on an adaptive gait for a quadruped walking robot under external forces," *Proc. IEEE Int. Conf. Robotics and Automation*, Albuquerque, New Mexico (April, 1997) pp. 2777–2782.
17. B. Lin and S. Song, "Dynamic modeling, stability and energy efficiency of a quadrupedal walking machine," *Proc. IEEE Int. Conf. Robotics and Automation*, Atlanta, Georgia (1993) pp. 367–373.
18. E. Papadopoulos and D. Rey, "A new measure of tipover stability margin for mobile manipulators," *Proc. IEEE Int. Conf. Robotics and Automation*, Minneapolis, Minnesota (April, 1996) pp. 3111–3116.
19. K. Yoneda and S. Hirose, "Three-dimensional stability criterion of integrated locomotion and manipulation," *Journal of Robotics and Mechatronics* **9**(4), 267–274 (1997).
20. E. Garcia, J. Estremera and P. Gonzalez de Santos, "A comparative study of stability margins for walking machines," *Robotica* **20** Part 6, 595–606 (2002).
21. D. Messuri, "Optimization of the locomotion of a legged vehicle with respect to maneuverability," *PhD thesis* (The Ohio State University, 1985).
22. P. Nagy, "An investigation of walker/terrain interaction," *PhD thesis*. (Carnegie Mellon University, 1991).
23. S. Hirose, H. Tsukagoshi and K. Yoneda, "Normalized energy stability margin: Generalized stability criterion for walking vehicles," *Proc. Int. Conf. Climbing and Walking Robots* Brussels, Belgium (November, 1998) pp. 71–76.
24. A. Ghasempoor and N. Sepehri, "A measure of stability for mobile manipulators with application to heavy-duty hydraulic machines," *ASME Journal of Dynamic Systems, Measurement and Control* **120**, 360–370 (1998).
25. Yobotics Inc., Boston, MA., *Yobotics! Simulation Construction Set: Users Guide, 2002*. Available: http://www.yobotics.com/.
26. E. Garcia, J. Galvez and P. Gonzalez de Santos, "A mathematical model for the real-time control of the SILO4 leg," *Proc. Int. Conf. Climbing and Walking Robots*, Madrid, Spain (October, 2000) pp. 447–460.
27. P. Gonzalez de Santos and M. Jimenez, "Generation of discontinuous gaits for quadruped walking machines," *Journal of Robotic Systems* **12**(9), 599–611 (1995).